202 W all-polarization-maintaining single-frequency fiber amplifier at C band

Jiehao Wang(王洁浩)[1,2,3], Zaiyuan Wang(王在渊)[1,2,3,4], Yuhang Li(李宇航)[1,2,3*] and Qiang Liu(柳强)[1,2,3]**

[1]Department of Precision Instrument, Tsinghua University, Beijing 100084, China
[2]State Key Laboratory of Precision Space-time Information Sensing Technology, Beijing 100084, China
[3]Key Laboratory of Photonic Control Technology, Ministry of Education, Tsinghua University, Beijing 100084, China
[4]Ordnance Sergeant College of Army Engineering University, Wuhan 430075, China
*Corresponding author: liyuhang@mail.tsinghua.edu.cn; **Corresponding author: qiangliu@mail.tsinghua.edu.cn

We demonstrate a 202 W all polarization-maintaining (PM) single-frequency fiber amplifier operating at C band. Simulations show that the length of the output fiber pigtail following the gain fiber critically has great impact on the stimulated Brillouin scattering (SBS), posing a major obstacle for high-power single-frequency amplification. Optimizing the length to suppress the backward SBS by ~ 10 dB, we experimentally achieved a maximum output power of 202 W, yielding an optical-to-optical efficiency of 42%. The signal-to-noise ratio (SNR) of signal light, relative to ASE in Er^{3+} and Yb^{3+} bands, was measured to be 23 dB and 32 dB, respectively, and they can be further improved by ASE suppression and filtering techniques during amplification. To the best of our knowledge, this is the all-PM single-frequency fiber amplifier with the highest power reported in the C band.
Keywords: EYDF amplifier, high power, single-frequency, SBS suppression.

1. Introduction

Featured with large optical gain, high efficiency, compact size, and high mechanical stability and reliability, fiber lasers have surpassed traditional solid-state lasers in popularity and have emerged as reliable sources across diverse fields, including industrial manufacturing [1], laser marking and engraving, precise spectroscopy [2], environmental monitoring and pollution control [3]. Notably, in the realm of gravitational wave detection, high power, low-noise and narrow-linewidth lasers constitute the most critical components of the detection system, ensuring adequate sensitivity amidst significant losses incurred over long transmission distances [4]. As the light source for the first-generation gravitational wave detector (GWD), 1μm fiber lasers based on Yb-doped fiber have attracted considerable attention in recent years. [5-8] However, 1 μm lasers couldn't pass through the silicon substrate which exhibit lower thermal noise when operating at cryogenic temperatures. Thus, researchers have turned their focus towards high-power low-noise single-frequency lasers operating in 1.5 μm and 2 μm bands, aiming at improving the gravitational wave detection sensitivity [9-12].

Well-established erbium-ytterbium co-doped fibers (EYDFs) are adopted to high-power low-noise amplification at C band, and the output power of single-frequency fiber lasers, which have ever-expanding applications, has continued to grow. In traditional EYDF amplifier schemes utilizing 976 nm laser diodes, Yb-band amplified spontaneous emission (ASE) is detrimental, prompting the development of pumping schemes which is off-resonant in the Yb^{3+} absorption band. In 2021, D. Darwich et al. reported a 10 W all-fiber laser system with an ultralow-intensity noise of -160 dBc/Hz beyond 200 kHz [13]. They pointed out that the pump had a major impact on intensity noise at low frequencies, and they employed a 940 nm pump to suppress ASE for a low noise operation. X. Chen et al. achieved a 59.1 W single-frequency output with 90% efficiency at 1560 nm using 1480 nm pump [14]. D. Varona et al. reported a 111 W 1.5 μm single-frequency fiber laser with polarization extinction ratio of 13dB [15]. Similarly, D. Creeden demonstrated an average output power of 207 W, accompanied by a linewidth of 540 Hz and a slope efficiency of 50.5% in a large-mode-area (LMA) Er-Yb fiber [16]. Although no ASE was observed on the optical spectrometer, the SBS limited the further enhancements.

Unfortunately, the PM gain fibers exhibit lower efficiency and nonlinear effect threshold compared to ordinary single-mode (SM) fiber [17], resulting in a much lower output power for polarization-maintaining fiber amplifiers compared to the works mentioned above. X. Bai et al. reported an all-fiber single-frequency master oscillator power amplifier (MOPA) at 1550 nm with the output power of 56.4 W and the slope efficiency of only 37% in 2015 [18]. P. Booker et al. presented a 110 W 2-stage single-frequency Er-Yb fiber amplifier at 1556 nm [19]. The RIN was 10^{-3}/Hz$^{-1/2}$ at 1 Hz and decreased to 10^{-6}/Hz$^{-1/2}$ at 100 kHz. The performance of noise is also affected by the pump when the output power above 50 W. In 2022, J. Huang et al. demonstrated an all-PM-fiber single-frequency narrow-linewidth laser operating at 1560 nm with 102 W output power and 40.6% slope efficiency [20]. This performance is still inadequate for applications such as gravitational wave detection. To meet the escalating detection requirements, addressing the issue of SBS during power amplification is paramount, particularly in all-PM fiber systems.

To alleviate the SBS effect, previous works typically focused on optimizing the length of the gain fiber while neglecting the impact of the passive fiber. In this letter, we present the design of a polarization-maintaining all-fiber C band laser amplifier based on a MOPA configuration. Guided by mathematical simulations, we investigated the physical mechanisms of ASE and SBS. Experimentally, we increased the threshold power of SBS by shortening the length of passive fiber pigtail following the gain fiber. Eventually, we decreased the SBS power by 10 dB and achieved a 202 W all-polarization-maintaining single-frequency fiber amplifier.

2. Nonlinear effect suppression scheme

Regarding laser power amplification, ASE has consistently emerged as a pivotal challenge in mitigating power enhancement. Furthermore, in single-frequency laser systems, SBS is equally, if not more, crucial than ASE [21]. In order to mitigate these nonlinear effects, we conducted a detailed analysis of each other and proposed corresponding strategies.

2.1. ASE

It is well-known that the absorption capacity of erbium particles is weak for pump light, and a significant concentration of doped particles often tends to cluster. This issue can be effectively addressed through Er-Yb co-doping. Fig. 1 illustrates the energy level diagram of the co-doped fibers. The Yb ions can efficiently absorb the pump energy and transfer it to erbium particles via cross relaxation. The evolution of power can be mathematically represented by Eq. (1) to Eq. (3), while the process of energy transfer is delineated by Eq. (4) to Eq. (8) [22]:

$$\pm\frac{dP_p^{\pm}}{dz}=\left[\Gamma_p N_{Yb}(n_6\sigma_{65}^{Yb}-n_5\sigma_{56}^{Yb})-\Gamma_s N_{Er}n_1\sigma_{13}^{Er}-\alpha_p\right]P_p^{\pm} \quad (1)$$

$$\pm\frac{dP_s^{\pm}}{dz}=\left[\Gamma_s N_{Er}(n_2\sigma_{21}^{Er}-n_1\sigma_{12}^{Er})-\alpha_s\right]P_s^{\pm} \quad (2)$$

$$\pm\frac{dP_{ASE,\lambda}^{\pm}}{dz}=\left[\Gamma_s N_{Yb}(n_6\sigma_{65,\lambda}^{Yb}-n_5\sigma_{56,\lambda}^{Yb})-\alpha_\lambda\right]P_{ASE,\lambda}^{\pm} \quad (3)$$

$$\frac{\partial n_2}{\partial t}=-\frac{n_2}{\tau_{21}}+\frac{n_3}{\tau_{32}}+W_{12}n_1-W_{21}n_2-2C_{up}N_{Er}n_2^{\,2} \quad (4)$$

$$\frac{\partial n_3}{\partial t}=-\frac{n_3}{\tau_{32}}+W_{13}n_1+R_{61}N_{Yb}n_6n_1-R_{35}N_{Yb}n_3n_5+C_{up}N_{Er}n_2^{\,2} \quad (5)$$

$$\frac{\partial n_6}{\partial t}=-\frac{n_6}{\tau_{65}}+W_{56}n_5-W_{65}n_6-R_{61}N_{Er}n_6n_1+R_{35}N_{Er}n_3n_5 \quad (6)$$

$$n_1=1-n_2-n_3 \quad (7)$$

$$n_5=1-n_6 \quad (8)$$

where P_p is the pump power, P_s the seed power, $P_{ASE,\lambda}$ the ASE power in Yb^{3+} band at wavelength λ. n_i is the population density in the i-th energy level, W_{ij} the stimulated transfer rate from the energy level i to the energy level j, R_{ij} the energy transfer between Er^{3+} and Yb^{3+} ions, C_{up} is the up-conversion coefficient. Γ, σ, α are respectively overlap factor, cross section and loss of pump and seed. τ_{ij} is the lifetime of the i-th energy level with respect to the transition in the j-th energy level, t the time, z the distance. N_{Er} and N_{Yb} are the ion concentration of erbium and ytterbium.

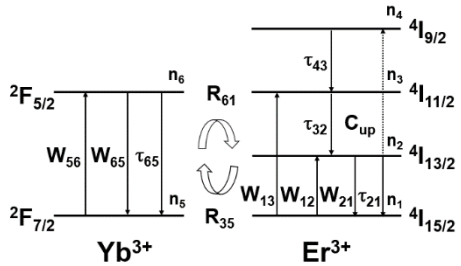

Fig. 1. Energy level diagram of Er^{3+} and Yb^{3+} ions.

Given the finite speed of energy transfer, scenarios where the signal power is insufficient or the pump absorption rate is excessively high can lead to the accumulation of Yb^{3+} ions in the upper level, ultimately producing ASE and potentially inducing parasitic oscillations. To suppress ASE, we adopted the off-resonant pumping approach, utilizing a pump diode with a wavelength of 915 nm, which exhibits a lower absorption coefficient compared to 976 nm. Fig. 2(a) presents the simulation result of Yb-ASE along the gain fiber at various pump wavelengths based on the aforementioned equations. It's evident that the ASE level are reduced when pumped at 915 nm. Furthermore, we investigated the impact of pumping direction. When employing the counter-propagation pumping scheme, the power distribution of both pump and signal remains consistent along the fiber. As the signal power increases, the more particles are consumed, thereby effectively suppressing the generation of ASE. The simulation results for different pump directions are depicted in Fig. 2(b).

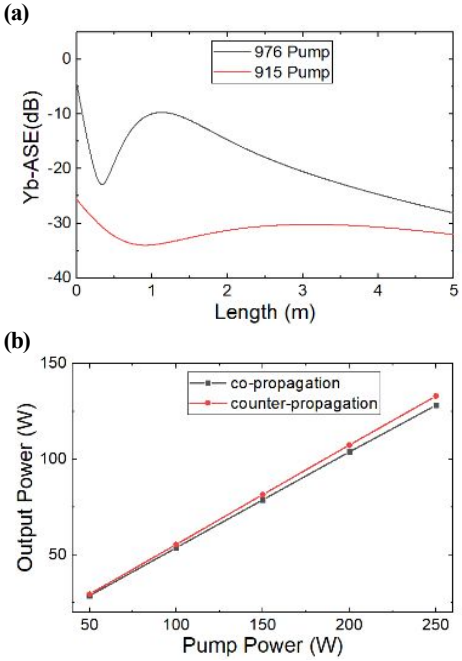

Fig. 2. Numerical simulation results of various pump schemes: (a) Different pump wavelengths; (b) Different pump directions

2.2. SBS

When high-power light propagates through the fiber, it experiences an increase in refractive index, leading to an electro-strictive effect. Consequently, a significant portion of the transmitted light is converted into backward scattered light. The equation of threshold power can be mathematically expressed as:

$$P_{th}=G\frac{AK}{g_B L}\frac{\Delta v_p+\Delta v_B}{\Delta v_B} \quad (9)$$

where G is the coefficient of threshold gain. Its value equals 21 in Smith theory model and 19 in Küng model [23]. K is the polarization dependent factor, which takes 1 and 2 for linear and random polarization. A and L are the effective area and propagation length of fiber. g is the peak value of Brillouin scattering. Δv_p is the linewidth of laser and Δv_B is the gain bandwidth of SBS. When the linewidth is more less than the gain bandwidth, the rightmost portion of the equation can be simplified to 1.

The simulation results for various parameters of the threshold power are presented in Fig. 3. From Fig. 3(a) and 3(b), it is evident that the threshold power increases as the length decreases or the area increases. Based on this observation, the core diameter of the gain fibers we selected is 25 μm. Additionally, to balance the pump absorption, typically 2.6 dB/m at 915 nm, with SBS suppression, a 5 m gain fiber in the amplifier is deemed an appropriate choice.

(a)

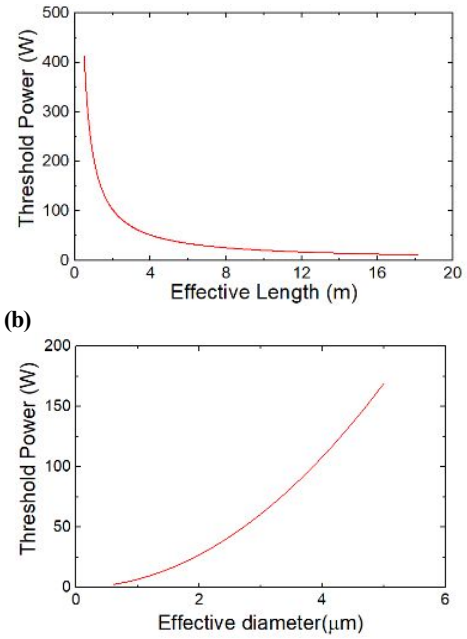

Fig. 3. Numerical simulation results of threshold power to: (a)Effective length; (b)Effective diameter.

Simultaneously, we noticed that despite the gain fiber being longer than the following passive fiber, the light power progressively increased along the gain fiber. This implies that the corresponding propagation length for higher power is shorter. But in the passive fiber section, the light power reaches its maximum and remains essentially constant, exhibiting a lower threshold power. We could optimize the amplifier configuration by shortening the passive fiber in the output section. It is noteworthy that the cladding power stripper would be placed before the gain fiber in the counter-propagation pumping scheme (as illustrated in Fig. 4). This configuration is advantageous as it allows for the use of the shortest pigtail behind the gain fiber, thereby enhancing the SBS threshold. Therefore, the counter-propagation pumping scheme we selected serves the dual purpose of inhibiting both ASE and SBS simultaneously. Considering that the change of temperature gradient of the fiber is also effective in suppressing SBS [24] and the main amplifier is mounted on a cooled plate, we could reduce the SBS gain by adjusting the plate temperature to alter the temperature gradient, while ensuring the normal operation of the device.

3. Experimental setup

Following the simulation and analysis, we have developed a single-frequency all-fiber amplifier, comprising a seed laser and two amplification stages. The schematic of the MOPA setup is shown in Fig. 4. The home-made seed laser delivers 14 mW at a wavelength of 1541 nm. Its linewidth is approximately 4 kHz measured by delayed self-heterodyne method. This seed is then amplified to 7 W by a commercial pre-amplifier module. An optical isolator is incorporated to mitigate possible damage caused by the backward light. To monitor the backward light, including normal end-face reflection and SBS, emanating from the main amplification stage, a coupler with a coupling ratio of 1 : 99 is reversely connected to the system. A mode field adapter is spliced after coupler to match the pigtails of subsequent devices. In the main amplification stage, a 915 nm multimode laser diode serves as the pump source and the residual pump is removed by a cladding light stripper. The gain fiber utilized is PLMA-EYDF-25/300, with a length of 5 m. Ultimately, the amplified signal light exits the fiber end-face with an angle of 8° to reduce the Fresnel reflection. The entire main amplification stage is temperature-controlled using a cooled plate to prevent heat accumulation-induced damage.

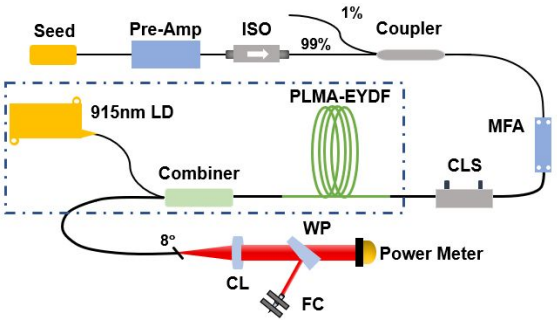

Fig. 4. Schematic of the experimental setup: Pre-Amp, pre-amplifier; ISO, optical isolator; MFA, mode field adapter; CLS, cladding light stripper; LD, laser diode; CL, collimating lens; WP: wedge prism; FC, fiber collimator.

Since the power range of optical instruments is limited, direct analysis of the output laser is infeasible except for the power meter. Therefore, a laser beam splitting-coupling system was designed and constructed for measurement purposes. We employed the end-face reflection of wedge prism for low-power splitting and carefully adjusted the angle of the fiber collimator to achieve coupling of space light into the fiber. Due to the large divergence angle of the direct laser output, a flat-convex lens is positioned in front of the wedge prism to collimate the beam and enhance the coupling efficiency. Both the wedge prism and lens are made of fused quartz, and the latter is coated with an anti-reflection film (AR@1000 nm~1600 nm) to minimize light reflection. Subsequent experimental results indicate that light at the 10 mW level can be collected using this method, fulfilling the requirements for measurement and analysis.

4. Results and Discussions

The output power of pre-amplifier is 7 W, but the actual input is only 5 W due to insertion loss in the fiber devices. When amplifying the laser without implementing any SBS suppression measures, the spectrum of backward light, as shown in Fig. 5, reveals a spike in the longer wavelength band when the output exceeds 30 W. The frequency difference between the two peaks is about 11 GHz, which corresponds to the frequency shift of Brillouin scattering. As the output power gradually increased to 130 W, the SBS peak rapidly rises and surpasses the signal peak by 20 dB, with an estimated actual SBS of about 2 W accordingly. This nonlinear increase in SBS becomes the primary limiting factor for further power amplification.

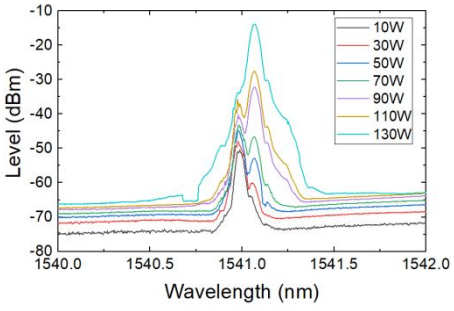

Fig. 5. Spectrum of backward light at different output powers.

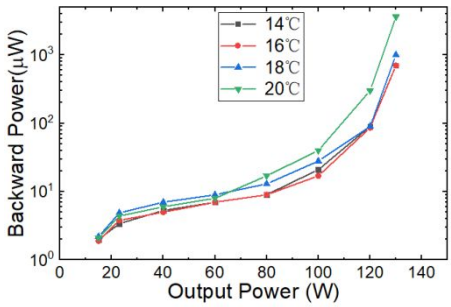

Fig. 6. Backward optical power at different cooled plate temperatures.

To alleviate this issue, we first investigated the influence of cooled plate temperature on SBS gain by comparing the backward optical power at the same fiber length and pump but varying temperatures. The results indicate that the SBS effect weakens as the temperature decreases above 16 ℃. The curves of backward optical power are plotted in Fig. 6. Considering that excessively low temperature could lead to additional energy consumption and potentially impact the performance of the pump diode, we determined that the optimal operating temperature for the cooled plate is 16 ℃. Subsequently, based on the simulations conducted in Part 2, we shortened the passive fiber behind the gain fiber. We progressively decreased the length of the fiber pigtail and recorded the backward power (including the reflection of fuse end and SBS) at different output powers. The backward power measured directly at the monitor end (representing only 1% of the total backward power) is shown in Fig. 7.

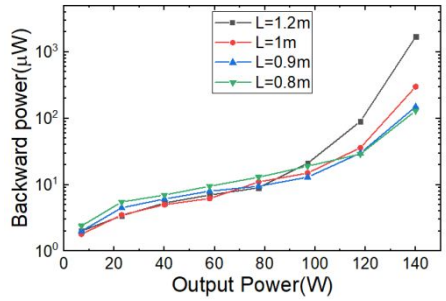

Fig. 7. Backward optical power at different passive fiber lengths.

When the fiber was reduced from 1.2 m to 1 m, the threshold power of SBS increased, accompanied by a rapid decrease in backward power from 1.7 mW to 0.3 mW. Upon further shortening the fiber by another 10 cm, the SBS further decreased, resulting in a backward power of only 0.15 mW. If the threshold power increases sufficiently, the SBS effect will not decrease significantly, explaining the near-identical curves observed for fiber lengths of 0.9 m and 0.8 m. at this point, it is plausible to assume that the backward light primarily consists of the reflected signal light.

With effective SBS suppression, the amplifier power could be further increased without significant SBS interference. Finally, we achieved an output power of 202 W at a pump power of 481 W, yielding an optical-to-optical efficiency of 42%. The linewidth was well-maintained to be about 4 kHz during the amplification, and no obvious broadening was observed. The total backward power was measured to be less than 0.2 W, indicating that the SBS was not a limiting factor in this scenario. The corresponding plots of output power versus pump power and efficiency are depicted in Fig. 8(a). The SNR we observed using the optical spectral analyzer (OSA) (as shown in Fig. 8(b)) was 23 dB, which is constrained by the SNR of pre-amplifier and the sensitivity of OSA. This SNR could be further enhanced through future optimizations of the pre-amplifier design, such as adopting a narrow-band filter and increasing the pre-amplifier power. In addition, we noticed a sharp increase in ASE in Yb-band, as illustrated in Fig. 8(c). This suggests that the ASE could induce parasitic oscillations and potentially damage the system with further increase in pump power. This issue might be alleviated by enhancing the pre-amplifier power and improving splicing quality. Alternatively, splicing a section of ytterbium-doped fiber before or after the gain fiber section to absorb ASE in the 1 μm band also presents a promising solution [25]. However, the length and splicing quality of this section must be optimized.

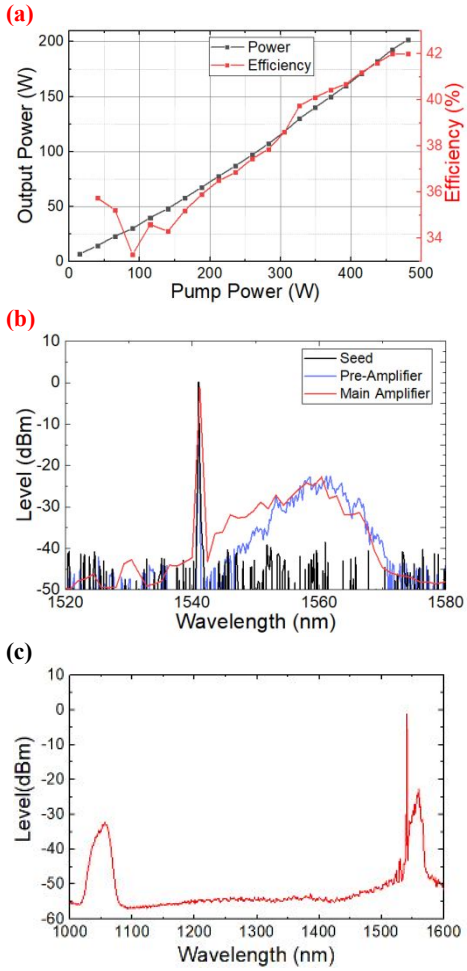

Fig. 8. (a) Output power; (b) Optical spectrum of signal light for the seed, pre-amplifier and main amplifier, respectively; (c)Output spectrum of signal light and ASE.

5. Conclusion

In this work, we demonstrated an all-fiber polarization-maintaining fiber laser amplifier operating at C band. Off-resonant and counter-propagation pumping schemes were employed to reduce the ASE level in Yb band by utilizing a 915 nm diode. Notably, we found that the length of passive fiber following the gain fiber played a crucial role in SBS suppression, thereby

limiting the maximum amplifier output power. By reducing the passive pigtail length to approximately 0.4 m, we achieved a single-frequency amplification output power of about 202 W at 1541 nm, with an optical-to-optical efficiency was 42%, and a SNR exceeding 20 dB, currently limited by the SNR of the commercial pre-amplifier. Therefore , we believe that a polarization-maintaining single-frequency fiber laser amplifiers with a significantly higher SNR can be realized by improving the performance of pre-amplifier via narrowband filtering and necessary optimization. With the help of noise suppression techniques, such as active feedback and second-harmonic generation in passive optical cavity [26,27], high-power low-noise single-frequency fiber amplifier would be very promising in applications in high precision interferometry and gravitational wave detection.

Acknowledgement
This work was supported by the National Natural Science Foundation of China (Nos. U22A6003 and 62175122).

References.

1. L. D. Scintilla and L. Tricarico, "Fusion cutting of aluminum, magnesium, and titanium alloys using high-power fiber laser," Opt. Eng. **52**, 076115 (2013).
2. Y. Lu, Z. Yu, Z. Ju, X. Hu, M. Chen, and Z. Meng, "SNR dependence of measurement stability of heterodyne phase-sensitive optical time-domain reflectometry," Appl. Opt. **59**, 6333 (2020).
3. I. T. Sorokina and K. L. Vodopyanov, *Solid-state mid-infrared laser sources* (Springer, 2003).
4. M. Steinke, H. Tunnermann, V. Kuhn, T. Theeg, M. Karow, O. de Varona, P. Jahn, P. Booker, J. Neumann, P. Weßels, and D. Kracht, "Single-frequency fiber amplifiers for next-generation gravitational wave detectors," IEEE J. Sel. Top. Quantum Electron. **24**, 1(2017).
5. T. Theeg, H. Sayinc, J. Neumann, and D. Kracht, "All-fiber counter-propagation pumped single frequency amplifier stage with 300-W output power," IEEE Photon. Technol. Lett. **24**, 1864 (2012).
6. M. D. Mermelstein, K. Brar, M. J. Andrejco, A. D. Yablon, M. Fishteyn, C. Headley, and D. J. DiGiovanni, "All-fiber 194 W single-frequency single-mode Yb-doped master-oscillator power-amplifier," Proc. IEEE 382 (2007).
7. P. Ma, P. Zhou, Y. Ma, R. Su, X. Xu, and Z. Liu, "Single-frequency 332 W, linearly polarized Yb-doped all-fiber amplifier with near diffraction-limited beam quality," Appl. Opt. **52**, 4854 (2013).
8. L. Huang, H. Wu, R. Li, L. Li, P. Ma, X. Wang, J. Leng, and P. Zhou, "414 W near-diffraction-limited all-fiberized single-frequency polarization-maintained fiber amplifier," Opt. Lett. **42**, 1 (2017).
9. N. Jiao, R. Li, Y. Wang, W. Zhang, C. Zhang, L. Tian, and Y. Zheng, "Laser phase noise suppression and quadratures noise intercoupling in a mode cleaner," Opt Laser Technol. **154**, 108303 (2022).
10. R. Li, N. Jiao, B. An, Y. Wang, W. Li, L. Chen, L. Tian, and Y. Zheng, "Optimizing frequency noise calibration and manipulation in an active feedback control loop," Opt Laser Technol. **174**, 110617 (2024).
11. V. Kuhn, D. Kracht, J. Neumann, and P. Weßels, "Er-doped single-frequency photonic crystal fiber amplifier with 70 W of output power for gravitational wave detection," Proc. SPIE **8237**, 263 (2012).
12. Q. Zhang, Y. Hou, X. Wang, W. Song, X. Chen, W. Bin, J. Li, C. Zhao, and P. Wang, "5 W ultra-low-noise 2 μm single-frequency fiber laser for next-generation gravitational wave detectors," Opt. Lett. **45**, 4911 (2020).
13. D. Darwich, Y. V. Bardin, M. Goeppner, C. Dixneuf, G. Guiraud, N. Traynor, G. Santarelli, and A. Hilico, "Ultralow-intensity noise, 10 W all-fiber single-frequency tunable laser system around 1550 nm," Appl. Opt. **60**, 8550 (2021).
14. X. Cheng, Z. Lin, X. Yang, S. Cui, X. Zeng, H. Jiang, and Y. Feng, "High-power 1560 nm single-frequency erbium fiber amplifier core-pumped at 1480 nm," High Power Laser Sci. Eng. **10**, e3 (2022).
15. De Varona. Omar, et al, "Single-frequency fiber amplifier at 1.5 μm with 100 W in the linearly-polarized TEM 00 mode for next-generation gravitational wave detectors," Opt. Express. **25.21**, 24880(2017).
16. D. Creeden, H. Pretorius, J. Limongelli, S. D. Setzler, "Single frequency 1560nm Er:Yb fiber amplifier with 207W output power and 50.5% slope efficiency," Proc. SPIE **9728**, 97282L (2016);
17. Z Wang, B Shao, "Threshold analysis and experimental study of stimulated Brillouin scattering in fiber," Laser & Optoelectronics Progress. **48**, 54(2011).
18. X. Bai, Q. Sheng, H. Zhang, S. Fu, W. Shi, and J. Yao, "High-power all-fiber single-frequency erbium–ytterbium co-doped fiber master oscillator power amplifier," IEEE Photonics J. **7(6)**, 1-6 (2015).
19. P. Booker, O. De Varona, M. Steinke, P. Wessels, J. Neumann, and D. Kracht, "Two-stage fully monolithic single-frequency Er: Yb fiber amplifier at 1556 nm for next-generation of gravitational wave detectors, " Fiber Lasers XVIII: Technology and Systems. **11665**, 100-105 (2021).
20. J. Huang, Q. Zhao, J. Zheng, et al, "A 102 W high-power linearly-polarized all-fiber single-frequency laser at 1560 nm," Photonics. **9(6)**, 396(2022).
21. C. Li, Y. Tao, M. Jiang, P. Ma, W. Liu, R. Su, J. Xu, J. Leng, and P. Zhou, "High-power single-frequency fiber amplifiers: progress and challenge [Invited]," Chin. Opt. Lett. **21**, 090002-(2023)
22. M. Steinke, J. Neumann, D. Kracht, and P. Wessels, "Gain dynamics in Er 3+: Yb 3+ co-doped fiber amplifiers," Opt. Express. **23**,14946 (2015).
23. R. G. Smith, "Optical power handling capacity of low loss optical fibers as determined by stimulated Raman and Brillouin scattering," Appl. Opt. **11**, 2489(1972).
24. S. Jeong, et al, "Characteristics of Stimulated Brillouin Scattering Suppression in High-Power Fiber Lasers Using Temperature Gradients," Korean Journal of Optics and Photonics. **30**,167(2019).
25. W. Li, Q. Qiu, L. Yu, Z. Gu, Le He, S. Liu, X. Yin, X. Zhao, J. Peng, H. Li, Y. Xing, Y. Chu, N. Dai, and J. Li, "Er/Yb co-doped 345-W all-fiber laser at 1535 nm using hybrid fiber, " Opt. Lett. **48**, 3027 (2023)
26. N. Jiao, R. Li, B. An, J. Wang, L. Chen, Y. Wang, and Y. Zheng, "Passive laser power stabilization in a broadband noise spectrum via a second-harmonic generator, " Opt. Lett. **49(13)**, 3568-3571 (2024).
27. L. Gao, L. Zheng, B. Lu, S. Shi, L. Tian, and Y. Zheng, "Generation of squeezed vacuum state in the millihertz frequency band," Light Sci. Appl. **13(1)**, 294 (2024).